Theor Chem Acc (2002) 108:12–20
DOI 10.1007/s00214-002-0350-1

Theoretical
Chemistry Accounts

Regular article

An atom-in-molecules and electron-localization-function study of the interaction between O_2 and $V_xO_y^+/V_xO_y$ ($x = 1, 2$, $y = 1$–5) clusters

M. Calatayud[1], **S. Berski**[1,2], **A. Beltran**[1], **J. Andrés**[1]

[1] Departament de Ciències Experimentals, Universitat Jaume I, P.O. Box 224, 12080 Castelló, Spain
[2] Faculty of Chemistry, University of Wroclaw, F. Joliot-Curie 14, 50-383 Wroclaw, Poland

Received: 15 October 2001 / Accepted: 30 January 2002 / Published online: 24 June 2002

Abstract. The most stable structures of $V_xO_y^+/V_xO_y$ ($x = 1, 2$, $y = 1$–5) clusters and their interaction with O_2 are determined by density functional calculations, the B3LYP functional with the 6-31G* basis set. The nature of the bonding of these clusters and the interaction with O_2 have been studied by topological analysis in the framework of both the atoms-in-molecules theory of Bader and the Becke–Edgecombe electron localization function. Bond critical points are localized by means of the analysis of the electron density gradient field, $\nabla\rho(\mathbf{r})$, and the electron localization function gradient field, $\nabla\eta(\mathbf{r})$. The values of the electron density properties, i.e., electron density, $\rho(\mathbf{r})$, Laplacian of the electron density, $\nabla^2\rho(\mathbf{r})$, and electron localization function, $\eta(\mathbf{r})$, allow the nature of the bonds to be characterized, and linear correlation is found for the results obtained in both gradient fields. Vanadium-oxygen interactions are characterized as unshared-electron interactions, and linear correlation is observed between the electron density properties and the V–O bond length. In contrast, O_2 units involve typical shared-electron interactions, as for the dioxygen molecule. Four different vanadium–oxygen interactions are found and characterized: a molecular O_2 interaction, a peroxo O_2^{2-} interaction, a superoxo O_2^- interaction and a side-on O_2^- interaction.

Key words: Vanadium oxides – Clusters – Bonding-electron localization function – Topological analysis

1 Introduction

Small metal oxide clusters nowadays find applications in many technological fields [1, 2, 3]. They constitute the building blocks of cluster-assembled materials, and their physical and chemical behavior exhibit strong dependence on their structure and size. Most of the experimental investigations have been devoted to the production and fragmentation of cluster ions in the gas phase with the aid of beam techniques [4, 5, 6, 7, 8]. In these experiments, a metal sample is ablated in a gas carrier flow with small amounts of oxidizer gas added, and plasma reactions take place. As a result, clusters of various sizes are produced and characterized on the basis of their stoichiometry. Most information on the structure of small clusters is obtained from analyzing the cluster size distribution by mass spectroscopy, rending chemical reactivity and ion mobility studies by means of photoelectron and IR spectroscopy [9, 10, 11]. However, characterization of the structure for the different clusters remains a challenge for experimentalists.

The vanadium oxide cluster family has been obtained and characterized experimentally by Bell and coworkers [12, 13, 14, 15], while Foltin et al. [16] studied their growth dynamics. A strong dependence of the cluster stability on the oxygen/vanadium ratio is found, leading to different cluster distributions for cationic and neutral systems. Systematic studies on this problem are helpful and a theoretical analysis can therefore be crucial in the understanding of their structure and electronic properties. The study of $V_xO_y^+$ and V_xO_y clusters is part of a broader program directed to understanding the physical and chemical properties of small oxide clusters by means of quantum-mechanical calculations [17, 18, 19, 20]. Our previous studies on this family of clusters have provided geometrical parameters, relative energy, fragmentation channels, vibrational data and vanadium-oxygen bonding descriptions [21, 22, 23]. However, some fundamental aspects remain to be studied, such as the factors that affect the strength and structure of the interaction between different vanadium oxide stoichiometries and molecular oxygen. Here, we attempt to reveal the nature of the interaction between $V_xO_y^+/V_xO_y$ with molecular oxygen by means of the atoms in molecules (AIM) and electron localization function (ELF) topological analysis. The layout o is as follows. The description of the computational procedure is presented in Sect. 2, together with a brief formulation of the AIM and ELF analysis of bonding. The results are presented and discussed in Sect. 3. Finally, the conclusions are given in Sect. 4.

Correspondence to: J. Andrés
e-mail: andres@exp.uji.es

2 Computational methodologies and model systems

The structures were optimized at the density functional level (DFT) using the B3LYP hybrid method [24, 25] implemented in the Gaussian94 program package [26]. The DFT scheme has been shown to correctly describe transition metals [21, 22, 23, 27, 28, 29, 30]. The wavefunctions were calculated at the restricted Hartree–Fock (HF) or unrestricted HF levels with a 6-31G* basis set developed by Rassolov et al. [31]. The nature of the stationary points was tested with frequency calculations and all the structures are characterized as minima. In the study of the binding energy between the different clusters and O_2, the basis set superposition error was corrected by the counterpoise procedure of Boys and Bernardi [32], and the relaxation of the fragments was also taken into account [33].

The AIM theory, developed by Bader and coworkers [34], allows a partition of the molecular space into atomic contributions through an analysis of the gradient vector field of the electron density. The presence of a (3, −1) critical point in the internuclear region connected to the nuclei by a unique pair of trajectories (a bond path) defines a bond. The nature of this bond can be described by the value of the electron density, $\rho(\mathbf{r})$, and the Laplacian of the electron density, $\nabla^2\rho(\mathbf{r})$. Thus, an unshared-electron interaction is characterized by low values of $\rho(\mathbf{r})$ and positive values of $\nabla^2\rho(\mathbf{r})$, whereas high values of $\rho(\mathbf{r})$ and negative $\nabla^2\rho(\mathbf{r})$ correspond to a shared-electron interaction. On the other hand, the topological analysis of the gradient vector field of the Becke and Edgecombe ELF function [35], as implemented by Silvi and coworkers [36, 37], involves molecular space partition into core and valence atomic attractors defining basins, the latter characterized by their synaptic order, i.e., the number of core attractors to which they are connected. Bonding is then defined on the basis of the interaction of these core and valence attractors: shared-electron interactions are characterized by polysynaptic valence bonding attractors lying between two or more core attractors. The ELF $\eta(\mathbf{r})$ is interpreted as a measure of the electron localization in atomic and molecular systems, as the conditional probability of finding two electrons with the same spin around a reference point [35]. Values below 0.5 correspond to totally delocalized electron density, while values above 0.5 indicate a localized character [38].

Bond critical points (BCP) in the gradient field of the electron density were primarily localized using "the AIM link" within Gaussian98 [39] and verified with the top_search tool of the Top_Mod suite of programs [40]. The attractors in the gradient field of the ELF were identified using the top_bas program and their positions were confirmed by means of top_search. The critical points (3, −1) in the gradient field of the ELF were localized using top_search. The calculation of the properties of all the critical points, i.e., the value of the electron density $\rho(\mathbf{r})$, Laplacian of the electron density $\nabla^2\rho(\mathbf{r})$ and ELF function $\eta(\mathbf{r})$ was performed by means of top_search. For the graphical representation of localization basins the SciAn program [41] was used.

The following systems were studied: VO^+, VO, VO_2^+, VO_2, $V_2O_4^+$, V_2O_4, $V_2O_5^+$ and V_2O_5. Previous experimental [12, 42, 43, 44] and theoretical [21, 22, 23, 42] studies demonstrate that they can be considered as stable species capable of incorporating molecular oxygen.

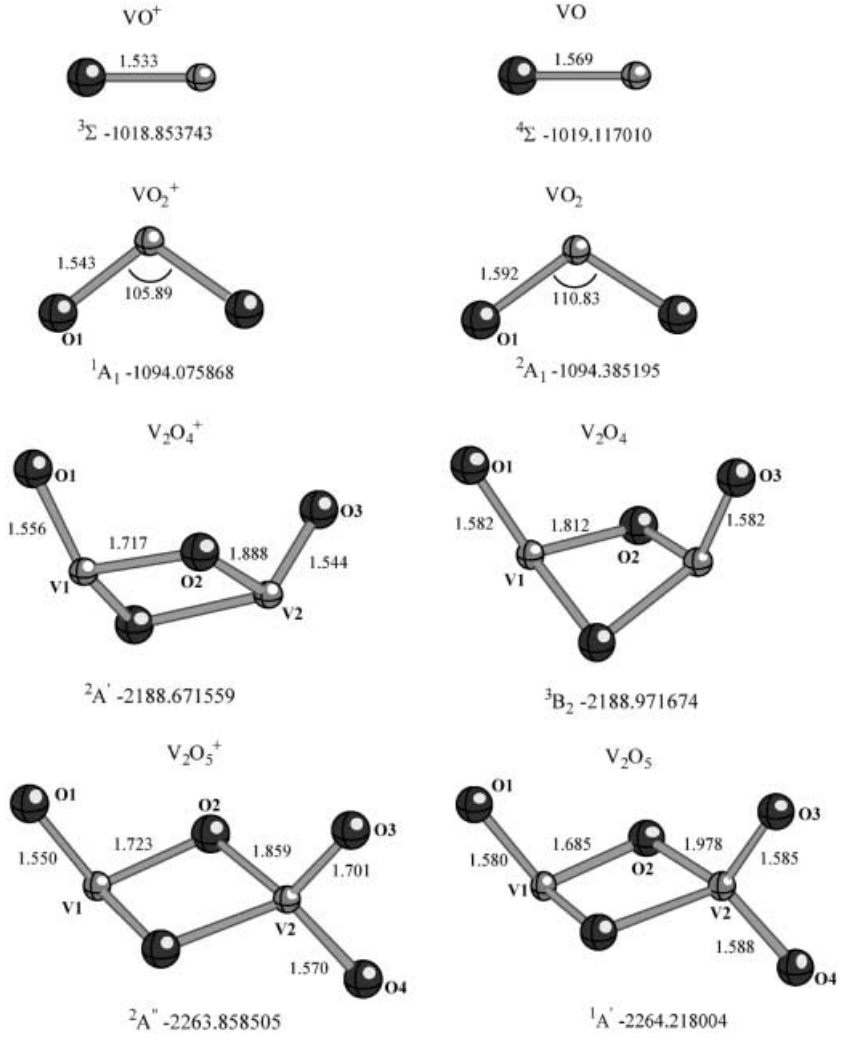

Fig. 1. Geometrical parameters and total energies for the most stable $V_xO_y^+$ and V_xO_y ($x = 1, 2$, $y = 1–5$) clusters (distances in angstroms and angles in degrees)

3 Results and discussion

In order to determine the nature of the bonding between $V_xO_y^+$ and V_xO_y ($x = 1, 2$, $y = 1$–5) clusters and an oxygen molecule, the clusters are characterized by means of the AIM and ELF analysis.

3.1 $V_xO_y^+$ and V_xO_y ($x = 1, 2$, $y = 1$–5) clusters

The geometrical parameters of the most stable structures for these stoichiometries are shown in Fig. 1 together with the total energy obtained in the calculations. Several structures involving cyclic and linear structures have been previously characterized at different electronic states [23]. The values of $\rho(\mathbf{r})$, $\nabla^2\rho(\mathbf{r})$, $\eta(\mathbf{r})$, at critical points (3, −1) in the electron density (AIM) and ELF gradient fields are collected in Table 1. The positions of the critical points are available upon request. The critical points are defined as those where the gradient of the field is zero, and the position of these points does not exactly coincide for the electron density and the ELF functions, as noticed by Bader et al. [45]. The study of a set of 20 V_xO_y and $V_xO_y^+$ clusters results in 58 values of $\rho(\mathbf{r})$, $\nabla^2\rho(\mathbf{r})$ and $\eta(\mathbf{r})$, obtained for the (3, −1) critical points in the gradient fields of both the electron density and the ELF function. The values of these magnitudes are depicted in Fig. 2, and linear correlation is observed between the values obtained in the gradient field of $\rho(\mathbf{r})$ and in the corresponding resulting from the gradient field of $\eta(\mathbf{r})$. In particular, the values of $\rho(\mathbf{r})$ and $\nabla^2\rho(\mathbf{r})$ are larger for the critical points located in the ELF gradient field, while the $\eta(\mathbf{r})$ value is larger for the critical points localized in the electron density gradient field. We conclude that the $\rho(\mathbf{r})$ values, showing a correlation of $R = 0.998$, and $\eta(\mathbf{r})$, with a correlation of 0.993, lead to similar results; $\nabla^2\rho(\mathbf{r})$ has a correlation of $R = 0.870$ probably due to the sensitivity of this function with regard to the position. The present relationship seems to be useful mainly for bonds possessing a large degree of ionicity because in such situations one systematically finds a (3, −1) critical point of the ELF close to a BCP of the electron density. From now on, the values corresponding to the BCP position calculated from the electron density gradient field will be used in the discussion. The $\rho(\mathbf{r})$ and $\nabla^2\rho(\mathbf{r})$ values are given in atomic units; the ELF function is adimensional.

The VO^+ ($^3\Sigma$) system has a BCP located between the vanadium and oxygen atom. The value of $\rho(\mathbf{r})$ at this point is 0.326 au, and $\nabla^2\rho(\mathbf{r})$ is 0.888 au, being an indication of an unshared-electron interaction. This is consistent with the ELF value of 0.431, below the localization reference value of 0.5. Similar values have been obtained for VO ($^4\Sigma$), VO_2^+ ($^1A_1$) and VO_2^+ ($^1A_1$) systems, and for structures possessing terminal oxygens, like $V_2O_4^+$ ($^2A'$), V_2O_4 ($^3B_2$) and V_2O_5 ($^1A'$). Thus, the electron density properties for the terminal oxygen–vanadium bonds are $\rho(\mathbf{r}) \approx 0.300$ au, $\nabla^2\rho(\mathbf{r}) \approx 0.900$ au and $\eta(\mathbf{r}) \approx 0.400$. Only $V_2O_5^+$ ($^2A''$) shows smaller values associated with the longest terminal oxygen–vanadium bond. This particular bond corresponds to an oxidation state of −1 for the oxygen atom, instead of the expected value of −2.

The structures possessing a four-membered cyclic V_2O_2 have the smallest values for the density properties

Table 1. Properties of the (3, −1) critical points localized in the gradient fields of the electron density (atoms in molecules, *AIM*) and electron localization function (*ELF*) for the most stable systems: electron density, $\rho(\mathbf{r})$ (atomic units), Laplacian of the electron density, $\nabla^2\rho(\mathbf{r})$ (atomic units), and ELF function, $\eta(\mathbf{r})$. The positions of the bond critical points (*BCPs*) are available upon request

System	AIM			ELF		
	$\rho(\mathbf{r})$	$\nabla^2\rho(\mathbf{r})$	$\eta(\mathbf{r})$	$\rho(\mathbf{r})$	$\nabla^2\rho(\mathbf{r})$	$\eta(\mathbf{r})$
VO^+ ($^3\Sigma$)	0.326	0.888	0.431	0.337	1.180	0.404
VO ($^4\Sigma$)	0.294	0.897	0.400	0.303	1.135	0.376
VO_2^+ ($^1A_1$)	0.322	0.908	0.422	0.328	1.181	0.396
VO_2 ($^2A_1$)	0.277	0.992	0.357	0.280	1.194	0.336
$V_2O_4^+$ ($^2A'$)						
V1–O1	0.312	0.891	0.415	0.324	1.248	0.380
V1–O2	0.198	0.752	0.320	0.205	0.961	0.290
V2–O2	0.117	0.580	0.200	0.117	0.697	0.176
V2–O3	0.322	0.856	0.432	0.336	1.229	0.397
V_2O_4 ($^3B_2$)						
V1–O1	0.288	0.863	0.401	0.301	1.219	0.365
V1–O2	0.147	0.695	0.234	0.152	0.871	0.207
$V_2O_5^+$ ($^2A''$)						
V1–O1	0.317	0.886	0.421	0.329	1.246	0.386
V1–O2	0.194	0.746	0.314	0.198	0.934	0.287
V2–O2	0.129	0.602	0.227	0.134	0.751	0.201
V2–O3	0.210	0.755	0.339	0.221	1.040	0.300
V2–O4	0.300	0.872	0.409	0.315	1.264	0.370
V_2O_5 ($^1A'$)						
V1–O1	0.291	0.883	0.399	0.301	1.221	0.364
V1–O2	0.215	0.810	0.326	0.218	1.023	0.298
V2–O2	0.091	0.469	0.165	0.095	0.591	0.142
V2–O3	0.284	0.855	0.400	0.295	1.201	0.364
V2–O4	0.287	0.849	0.404	0.299	1.193	0.369

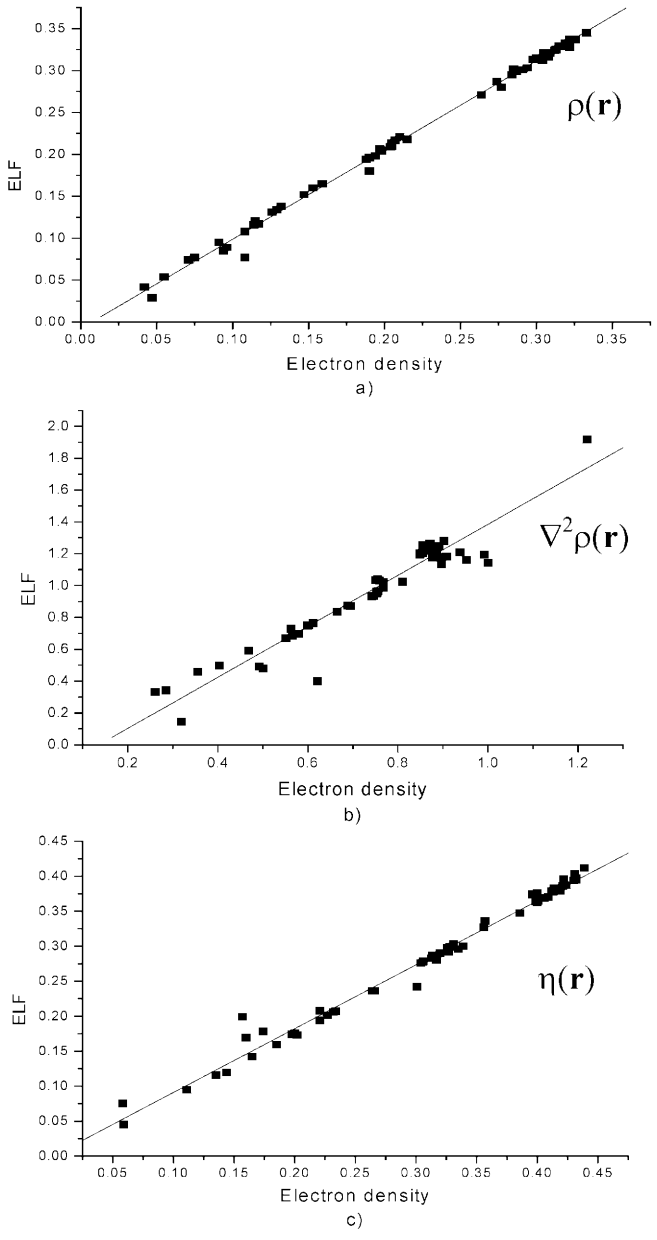

Fig. 2. Correlation between values of **a** the electron density, $\rho(\mathbf{r})$, in atomic units, **b** the Laplacian of the electron density, $\nabla^2\rho(\mathbf{r})$, in atomic units and **c** the electron localization function, $\eta(\mathbf{r})$. The magnitudes were computed for the (3, −1) critical points localized in the gradient fields of both the $\rho(\mathbf{r})$ and the $\eta(\mathbf{r})$, and the position does not always coincide (see text); however, linear correlation is observed

assigned to the oxygen ring–vanadium bond. Thus, values of $\rho(\mathbf{r})$ lower than 0.200 au, of $\nabla^2\rho(\mathbf{r})$ of the order of 0.700 au and of $\eta(\mathbf{r})$ around 0.300 are found for the cyclic system in $V_2O_4^+$ ($^2A'$), V_2O_4 ($^3B_2$), $V_2O_5^+$ ($^2A''$) and V_2O_5 ($^1A'$).

In all cases, the (3, −1) critical points located between the V and O atoms are characterized by a lack of electron pairing; consequently, an unshared-electron interaction exists for the V–O bonds. A dependence of the density properties on the V–O bond length is found, and is discussed later.

3.2 Interaction with O_2

Upon exposure of transition metals to O_2, several transition metal–O_2 interactions have been observed. Thus, molecular O_2, peroxo O_2^{2-} and superoxo O_2^- containing complexes species have been studied experimentally and theoretically from the point of view of geometry, energy and IR spectra [28, 42], as a result of the variety in the metal oxidation states. This work presents a detailed analysis of the O–O and V–O_2 bond properties within the AIM and ELF frameworks.

The geometry of the O_2 ($^3\Sigma_g$) molecule as well as the most stable structures for cationic and neutral O_2-containing clusters are depicted in Figs. 3 and 4. The binding energies of the V and O_2 fragments to form a V–O_2 complex are listed in Table 2. The calculated values of the binding energies range from –2.93 to 0.32 eV. With the exception of VO_4^+ ($^1A'$) model I and VO_4^+ ($^1A'$) model II clusters, the binding energies correspond to exothermic processes indicating the stability of the RV–O_2 bond, the most favorable interaction being the VO_2–O_2 one.

The electron density properties for these compounds are shown in Table 3. The O_2 ($^3\Sigma_g$) molecule is described in the AIM and ELF frameworks as follows. A (3, −1) critical point is located between the oxygen atoms according to the electron density gradient field analysis. This BCP is characterized by a $\rho(\mathbf{r})$ value of 0.518 au, a $\nabla^2\rho(\mathbf{r})$ value of −0.645 au and a $\eta(\mathbf{r})$ value of 0.807. These values, a high electron density, a negative Laplacian and $\eta > 0.5$, are typical for closed-shell interactions, as would be the case for the dioxygen molecule. The analysis of the ELF gradient field yields the same results, although the nature of the critical point is (3, −3). For closed-shell interactions in the ELF framework there are no bonding attractors between core attractors; therefore, (3, −1) critical points are used instead of (3, −3).

The VO_3^+ ($^1A'$) cluster is composed of a VO^+ unit and a side-on O_2 unit. The O_2 fragment is bonded to the vanadium center by means of two BCPs, with values of $\rho(\mathbf{r}) = 0.190$ au, $\nabla^2\rho(\mathbf{r}) = 1.000$au and $\eta(\mathbf{r}) = 0.221$. These values are characteristic of unshared-electron interactions, as for the rest of the V–O bonds. Along the O–O line, a BCP is found with $\rho(\mathbf{r}) = 0.308$ au, $\nabla^2\rho(\mathbf{r}) = 0.042$ au and $\eta(\mathbf{r}) = 0.673$. Despite the positive value of $\nabla^2\rho(\mathbf{r})$, the electron density properties indicate a shared-electron interaction for the O–O bond. In the ELF analysis, two monosynaptic attractors separated by the BCP appear in the line between the two oxygen atoms. The small monosynaptic basins are shown in the ELF isovalue picture in Fig. 5d. This type of bond is a "protocovalent" bond, and has been previously characterized for the F_2 molecule [46].

According to the side-on geometry of the O_2 unit, the interaction present in the VO_3^+ ($^1A'$) cluster can be classified as a peroxo one, whose electron density properties and ELF picture are characteristic of a protocovalent bond. This assignment is confirmed by the O–O distance in the range of 1.40 Å. A formal charge analysis, in which the vanadium atom is assumed to have an oxidation state of +5, and terminal oxygen −2,

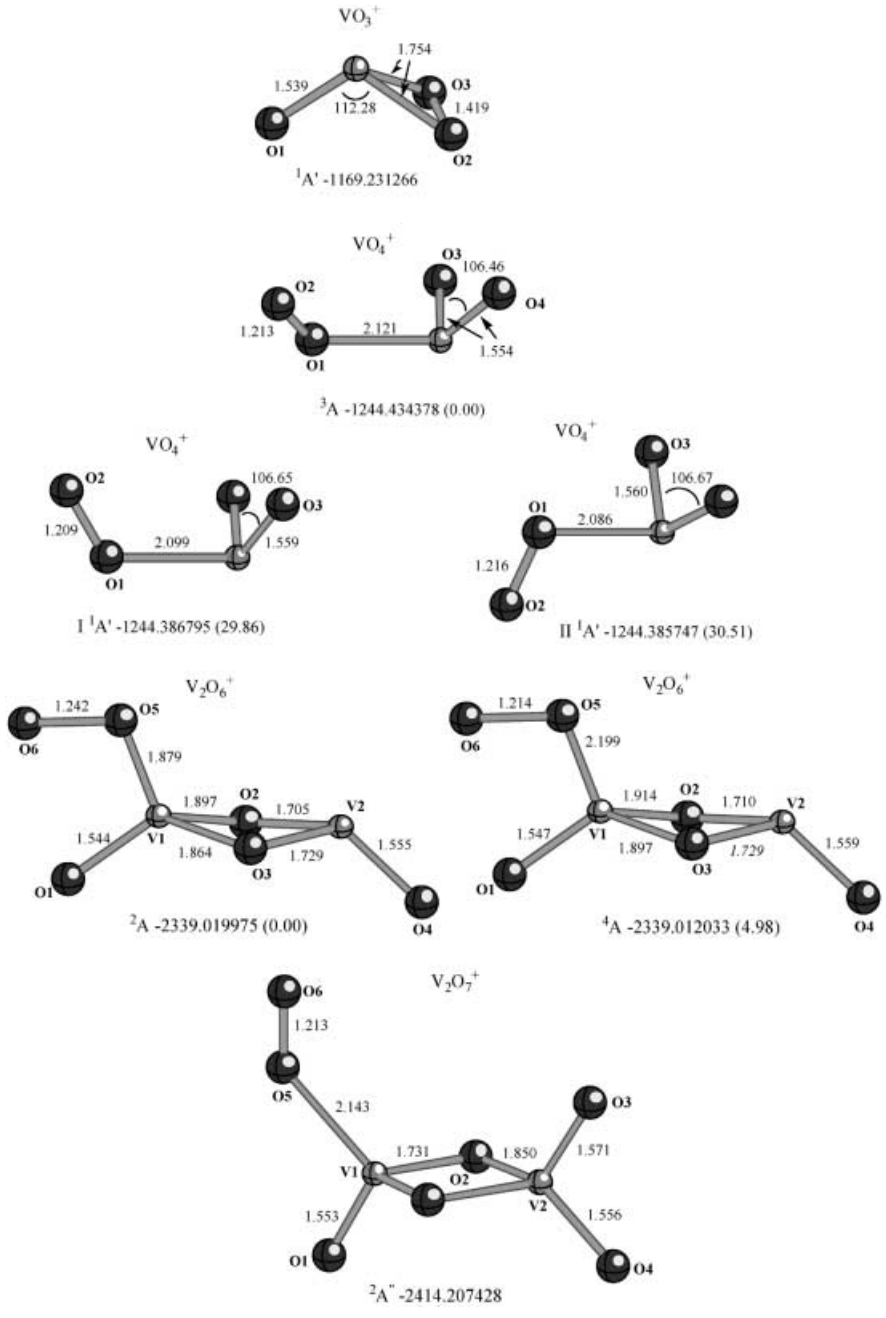

Fig. 3. Geometrical parameters, total energies and relative energies (in *parentheses*) for the cationic $V_xO_y^+$ ($x = 1, 2$, $y = 1-7$) clusters (distances in angstroms, angles in degrees, energies in kilocalories per mole)

renders a formal charge of −2 for the O_2 unit. The Bader charges analysis, obtained from the integration of the electron density over the ELF basins, renders a charge transfer of 0.44 electrons to the dioxygen fragment.

The most stable VO_4^+ (^{3}A) cluster is formed of a VO_2^+ unit and an end-on O_2 unit. The short V–O bonds as well as the long V–O_2 distance are characterized as electrostatic interactions in terms of the AIM and ELF analysis. The O_2 unit, however, shows typical shared-electron interactions with values of $\rho(\mathbf{r}) = 0.516$ au, $\nabla^2\rho(\mathbf{r}) = -0.615$ au and $\eta(\mathbf{r}) = 0.807$ at the BCP, in the range of the isolated O_2 molecule description. The ELF isovalue picture (Fig. 5a) shows a symmetric disynaptic basin between two almost identical oxygen valence basins. From this point of view, this description would correspond to a molecular O_2 interaction with the cationic fragment. A Bader charge analysis gives a negligible charge of 0.06 electrons for the O_2 unit, which is in agreement with a formal charge of 0 for the dioxygen moiety. The molecular O_2 interaction is also found for the two isomeric forms of VO_4^+ (^{1}A′) as well as for VO_4 (^{4}A), $V_2O_6^+$ (^{4}A) and $V_2O_7^+$ (^{2}A″).

On the other hand, $V_2O_6^+$ (^{2}A) involves a different interaction of a $V_2O_4^+$ cluster with an end-on O_2 unit: a BCP is found between the two oxygen atoms with $\rho(\mathbf{r}) = 0.474$ au, $\nabla^2\rho(\mathbf{r}) = -0.485$ au and $\eta(\mathbf{r}) = 0.795$. These values are smaller than the previously reported ones, a superoxo O_2^- unit is proposed for this structure. The ELF isovalue picture shows an asymmetric disynaptic basin between two oxygen valence basins, one of

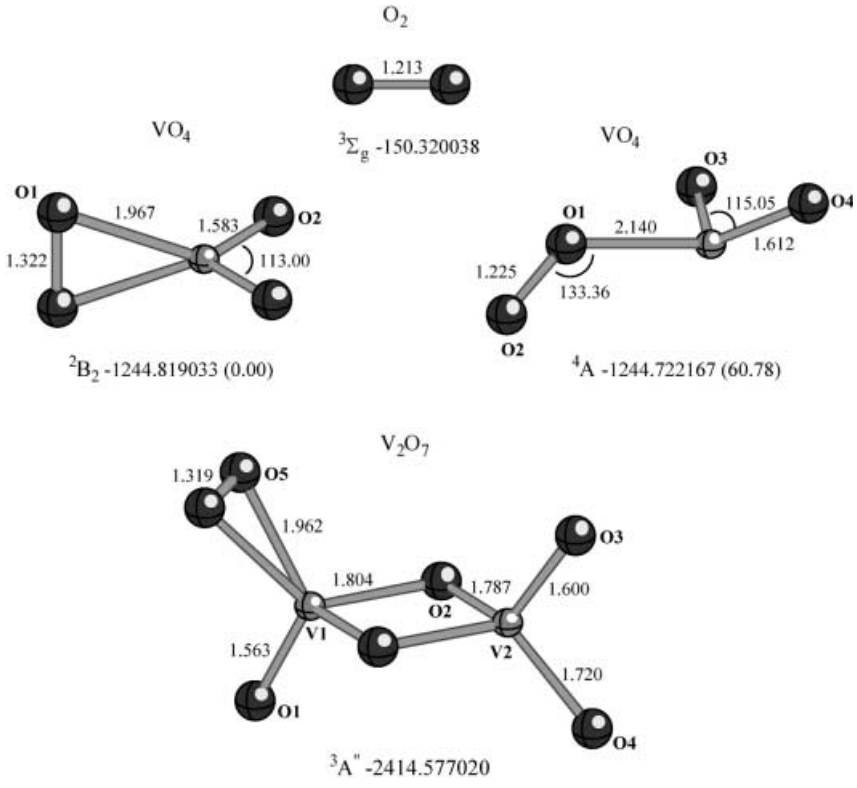

Fig. 4. Geometrical parameters, total energies and relative energies (in *parentheses*) for the neutral V_xO_y ($x = 1, 2$, $y = 1$–7) clusters as well as the O_2 molecule (distances in angstroms, angles in degrees, energies in kilocalories per mole)

Table 2. Binding energy (electron volts) for the $V_xO_y^+ - O_2$ and $V_xO_y - O_2$ ($x = 1, 2, y = 1$–5) clusters. Basis set superposition error and fragments relaxation were considered (see text)

System	Interaction energy
$VO^+(^3\Sigma) + O_2(^3\Sigma_g) \rightarrow VO_3^+(^1A')$	−1.36
$VO_2^+(^1A_1) + O_2(^3\Sigma_g) \rightarrow VO_4^+(^3A)$	−1.03
$VO_2^+(^1A_1) + O_2(^3\Sigma_g) \rightarrow VO_4^+(^1A')$I	0.28
$VO_2^+(^1A_1) + O_2(^3\Sigma_g) \rightarrow VO_4^+(^1A')$II	0.32
$VO_2(^2A_1) + O_2(^3\Sigma_g) \rightarrow VO_4(^2B_2)$	−2.93
$VO_2(^2A_1) + O_2(^3\Sigma_g) \rightarrow VO_4(^4A)$	−0.39
$V_2O_4^+(^2A') + O_2(^3\Sigma_g) \rightarrow V_2O_6^+(^2A)$	−0.72
$V_2O_4^+(^2A') + O_2(^3\Sigma_g) \rightarrow V_2O_6^+(^4A)$	−0.52
$V_2O_5^+(^2A'') + O_2(^3\Sigma_g) \rightarrow V_2O_7^+(^2A)$	−0.77
$V_2O_5(^1A') + O_2(^3\Sigma_g) \rightarrow V_2O_7(^3A)$	−0.98

them clearly smaller than the other because of the interaction with the vanadium center (Fig. 5b). Besides the interatomic O–O distance, a charge analysis supports this assignment: an O_2 with a formal charge of −1 compensates two vanadium atoms +5 and four oxygens −2 to give $V_2O_6^+$. The calculated Bader charges render a charge transfer of 0.33 electrons to the O_2 unit. Note the large alteration of the bond length on going from the ^2A to the ^4A electronic state (0.32Å), which induces a dramatic decrease in the value of all the parameters for the V–O_2 BCP. According to these results, a superoxo species would be present for the doublet electronic state, while the quartet electronic state would present molecular O_2. The most stable neutral V_2O_6 (^3A) cluster, not presented here, does not show a O_2 unit but four terminal oxygens.

Another type of O_2 interaction has been found for VO_4 ($^2B_2$). In this system, the dioxygen molecule is oriented side on, as for the peroxo VO_3^+ ($^1A'$) cluster. However, only one attractor is found between the two oxygen atoms, instead of the two found for VO_3^+. The electron density properties at this BCP are closer to those of the superoxo fragments: $\rho(\mathbf{r}) = 0.390$ au, $\nabla^2\rho(\mathbf{r}) = -0.241$ au and $\eta(\mathbf{r}) = 0.753$, as well as the O–O bond length. The disynaptic basin in the ELF isovalue picture is symmetric and the oxygen valence basins are distorted toward the vanadium center. The Bader charges analysis renders a charge transfer of 0.48 electrons to the dioxygen unit, while a formal charge of −1 is expected. This interaction can be then considered as intermediate between the peroxo and superoxo ones. The same side-on O_2^- moiety is found in the V_2O_7 ($^3A''$) cluster.

The comparative study on other V–O bonds shows a regular dependence between values of the $\nabla^2\rho(\mathbf{r})$, $\rho(\mathbf{r})$ and $\eta(\mathbf{r})$ parameters and the bond lengths, and a detailed analysis has been carried out. The representation of a total of 58 points renders a linear dependence upon the V–O bond length. The correlation between $\nabla^2\rho(\mathbf{r})$ and the V–O bond length is shown in Fig. 6. Note the different families of points corresponding to short terminal oxygens, ring oxygens and long V–O_2 distances.

4 Conclusion

The conclusions of the present work can be summarized as follows:

1. For all pairs of V and O atoms in the V_xO_y and $V_xO_y^+$ clusters, usually described in the Lewis represen-

Table 3. Properties of the (3, −1) critical points localized in the gradient fields of the electron density (AIM) ELF. The positions of the BCPs are available upon request

System	AIM			ELF		
	$\rho(\mathbf{r})$	$\nabla^2\rho(\mathbf{r})$	$\eta(\mathbf{r})$	$\rho(\mathbf{r})$	$\nabla^2\rho(\mathbf{r})$	$\eta(\mathbf{r})$
O_2 ($^3\Sigma_g$)						
O–O	0.518	−0.645	0.807	0.518	−0.645	0.807[a]
VO_3^+ ($^1A'$)						
V–O1	0.285	1.220	0.301	0.302	1.917	0.242
V–O2	0.190	1.000	0.221	0.180	1.141	0.208
O2–O3	0.308	0.042	0.673	0.278	0.086	0.694
VO_4^+ (^3A)						
V–O1	0.053	0.318	0.086	0.055	0.388	0.073
V–O3	0.313	0.868	0.423	0.321	1.188	0.392
O1–O2	0.516	−0.615	0.807	0.517	−0.620	0.808[a]
VO_4^+($^1A'$) I						
V–O1	0.075	0.404	0.135	0.077	0.498	0.116
V–O3	0.306	0.886	0.412	0.316	1.218	0.379
O1–O2	0.509	−0.558	0.796	0.519	−0.617	0.799[a]
VO_4^+ ($^1A'$) II						
V–O1	0.071	0.355	0.144	0.074	0.458	0.120
V–O3	0.308	0.883	0.414	0.316	1.204	0.383
O1–O2	0.516	−0.588	0.801	0.529	−0.664	0.804[a]
VO_4 ($^2B_2$)						
V–O1	0.094	0.501	0.160	0.085	0.479	0.169
V–O2	0.289	0.849	0.406	0.301	1.203	0.369
O1–O1	0.390	−0.241	0.753	0.390	−0.241	0.753[a]
VO_4 (^4A)						
V–O1	0.047	0.320	0.058	0.029	0.145	0.075
V–O3	0.264	0.938	0.356	0.271	1.208	0.327
O1–O2	0.501	−0.564	0.802	0.503	−0.572	0.802[a]
$V_2O_6^+$ (^2A)						
V1–O1	0.322	0.856	0.432	0.337	1.244	0.395
V1–O2	0.126	0.599	0.221	0.131	0.748	0.194
V1–O3	0.115	0.562	0.202	0.121	0.728	0.173
V1–O5	0.108	0.621	0.157	0.077	0.399	0.199
V2–O2	0.190	0.754	0.304	0.196	0.953	0.276
V2–O3	0.205	0.753	0.331	0.210	0.952	0.303
V2–O4	0.313	0.888	0.417	0.325	1.244	0.382
O5–O6	0.474	−0.485	0.795	0.494	−0.575	0.803[a]
$V_2O_6^+$ (^4A)						
V1–O1	0.319	0.855	0.430	0.333	1.229	0.394
V1–O2	0.114	0.566	0.198	0.116	0.683	0.174
V1–O3	0.108	0.551	0.185	0.108	0.668	0.159
V1–O5	0.042	0.261	0.059	0.042	0.331	0.045
V2–O2	0.198	0.768	0.313	0.204	0.983	0.283
V2–O3	0.204	0.756	0.328	0.209	0.964	0.299
V2–O4	0.309	0.890	0.413	0.321	1.245	0.378
O5–O6	0.517	−0.615	0.807	0.518	−0.616	0.807[a]
$V_2O_7^+$ (^2A)						
V1–O1	0.315	0.866	0.424	0.329	1.239	0.387
V1–O2	0.188	0.742	0.306	0.194	0.932	0.278
V2–O2	0.132	0.612	0.232	0.138	0.765	0.206
V2–O3	0.299	0.871	0.409	0.313	1.261	0.370
V2–O4	0.207	0.751	0.335	0.217	1.033	0.296
V1–O5	0.055	0.285	0.111	0.054	0.343	0.095
O5–O6	0.516	−0.595	0.803	0.529	−0.667	0.807[a]
V_2O_7 (^3A)						
V1–O1	0.305	0.855	0.419	0.321	1.254	0.379
V1–O2	0.153	0.665	0.264	0.160	0.834	0.236
V2–O2	0.159	0.688	0.266	0.165	0.874	0.236
V2–O3	0.274	0.867	0.386	0.287	1.230	0.347
V2–O4	0.197	0.760	0.317	0.207	1.030	0.280
V1–O5	0.096	0.492	0.174	0.089	0.491	0.178
O5–O5	0.393	−0.248	0.753	0.392	−0.247	0.755

[a] The critical point is characterized as (3, −1) in the AIM analysis, but as (3, −3) in the ELF analysis

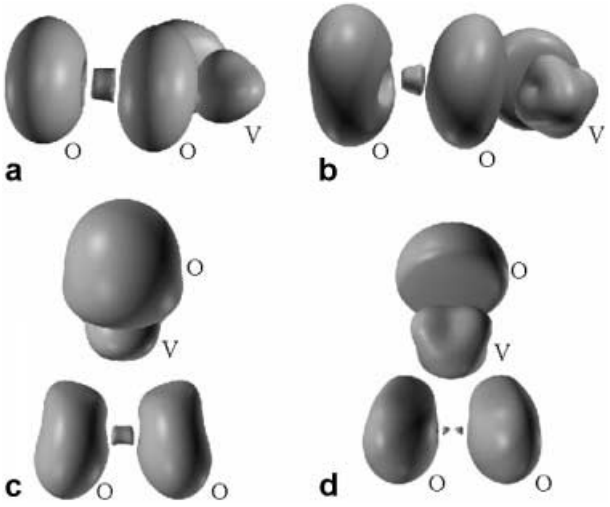

Fig. 5a–d. Electron localization function isosurfaces for the four different cluster–O_2 interactions. **a** Molecular O_2 interaction (η isovalue of 0.73). The oxygen valence basins are symmetric, as well as the disynaptic V(O,O) basin between them. **b** Superoxo O_2^- interaction (η isovalue of 0.73). The oxygen valence basin closest to the vanadium atom is slightly smaller than the other one. The disynaptic V(O,O) basin between them is distorted in the direction of the vanadium atom. **c** Side-on O_2^- interaction (η isovalue of 0.71). The two oxygen valence basins point to the vanadium atom and are slightly distorted. The disynaptic V(O,O) basin is symmetric. **d** Peroxo O_2^{2-} interaction (η isovalue of 0.686). The oxygen valence basins point to the vanadium atom. Two small monosynaptic basins appear instead of a monosynaptic one, indicating the presence of a protocovalent bond

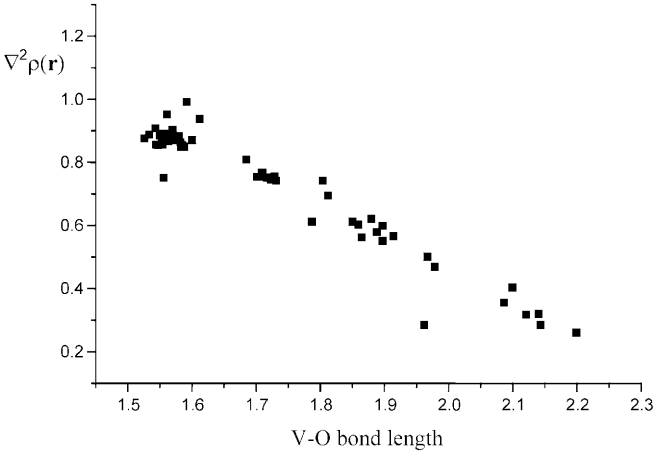

Fig. 6. Correlation between values of $\nabla^2\rho(\mathbf{r})$ and the V–O bond length (atomic units and angstroms, respectively)

tation by a chemical bond, localized bond paths and associated (3, −1) BCPs are found. According to Bader, the V–O interactions are classified as bonding interactions in the usual chemical sense of the word. The values of $\nabla^2\rho(\mathbf{r})$ are positive and closed-shell interactions are suggested. These interactions are dominated by the kinetic energy in the region of the BCP. The stability of the clusters results from electrostatic interactions among electronic charges separately concentrated within the atomic basins. In addition, the values of the electron density properties can be linearly correlated to the V–O distance.

2. A bonding interaction between oxygen atoms is observed for $VO_3^+(^1A')$, $VO_+(^3A)$, VO_4^+ $(^1A')$I, VO_+ $(^1A')$II, $VO_4(^2B_2)$, $VO_4(^4A)$, $V_2O_6^+$ (^2A), $V_2O_6^+(^4A)$, $V_2O_7^+(^2A)$ and $V_2O_7(^3A)$ clusters. These O–O bonds are characterized by bond paths with (3, −1) critical points in the $\rho(\mathbf{r})$ gradient field and have associated negative values of $\nabla^2\rho(\mathbf{r})$. With the exception of VO_3^+ $(^1A')$, there is a concentration of the electron density in the BCP region and bonds are thus formed owing to the pairing of the electron density.

3. Three previously recognized types of O–O bonds have been characterized by means of the topological analysis of the electron density and the ELF: molecular O_2, superoxo O_2^- and peroxo O_2^{2-}. In addition, an interaction exhibiting both peroxo and superoxo features has been characterized.

4. A molecular O_2 O–O bond exists in the VO_4^+ (^3A), VO_4^+ $(^1A')$ isomers I and II, VO_4 (^4A), $V_2O_6^+$ (^4A) and $V_2O_7^+$ (^2A) clusters. It is characterized by values of $\rho(\mathbf{r})$ around 0.50 au, $\nabla^2\rho(\mathbf{r})$ ranging from −0.564 to −0.615 au and $\eta(\mathbf{r})$ around 0.800. The ELF isovalue picture shows a symmetric disynaptic basin between two almost identical oxygen valence basins.

5. The superoxo O_2^- O–O bond exists in the $V_2O_6^+$ (^2A) molecule and is characterized by values of $\rho(\mathbf{r}) = 0.474$ au, $\nabla^2\rho(\mathbf{r}) = -0.485$ au and $\eta(\mathbf{r}) = 0.795$. The ELF isovalue picture is composed of an asymmetric disynaptic basin connected to the two distorted oxygen valence basins.

6. The side-on O_2 unit bond found in the VO_3^+ (^1A) molecule can be assigned to a peroxo interaction. It has electron density values of $\rho(\mathbf{r}) = 0.308$ au, $\nabla^2\rho(\mathbf{r}) = 0.042$ au and $\eta(\mathbf{r}) = 0.673$. Despite the positive value of $\nabla^2\rho(\mathbf{r})$, the presence of two attractors lying between the oxygen centers describes a shared-electron interaction corresponding to a protocovalent bond, as the ELF isovalue picture reflects.

7. The VO_4 $(^2B_2)$ and V_2O_7 (^3A) clusters present a side-on dioxygen with character intermediate between peroxo and superoxo interactions: $\rho(\mathbf{r}) \approx 0.390$ au, $\nabla^2\rho(\mathbf{r}) \approx -0.240$ au and $\eta(\mathbf{r}) = 0.753$. The ELF isovalue picture reveals a monosynaptic basin located between two equivalent oxygen valence basins distorted toward the vanadium center.

Acknowledgements. This work was supported by Fundació Caixa Castelló-Bancaixa (projecte P1A99-02). M.C. is grateful to Conselleria de Cultura, Educació i Ciència (Generalitat Valenciana) for a doctoral fellowship. S. B. thanks Fundació Caixa Castelló-Bancaixa for a visiting professor grant (year 2001). Computer facilities of the Servei d'Informàtica (Universitat Jaume I) are acknowledged.

References

1. Busca G, Lietti L, Ramis G, Berti F (1998) Appl Catal B 18: 1
2. Yamashita H, Harada M, Tanii A, Honda M, Takeuchi M, Ichihashi Y, Anpo M, Iwamoto N, Itoh N, Hirao T (2000) Catal Today 63: 63
3. Müller A, Das SK, Kuhlmann C, Bögge H, Schmidtmann MED, Krickemeyer E, Hormes J, Modrow H, Schindler S (2001) Chem Commun 7: 655

4. Kerns KP, Guo BC, Deng HT, Castleman AW Jr (1996) J Phys Chem 100: 16817
5. Fialko EF, Kikhtenko AV, Goncharov VB, Zamaraev KI (1997) J Phys Chem A 101: 8607
6. Persson JL, Andersson M, Holmgren L, Aklint T, Rosén A (1997) Chem Phys Lett 271: 61
7. Zhou M, Andrews L (1998) J Phys Chem A 102: 8252
8. Ding C-F, Yu Y, Jensen RH, Balfour WJ, Qian CXW (2000) Chem Phys Lett 331: 163
9. Castleman AW Jr, Bowen KH Jr (1996) Science 271: 920
10. Castleman AW Jr, Bowen KH Jr (1996) J Phys Chem 100: 12911
11. von Helden G, Kirilyuk A, van Heijnsbergen D, Sartakov B, Duncan MA, Meijer G (2000) Chem Phys 262: 31
12. Bell RC, Zemski KA, Kerns KP, Deng HT, Castleman AW Jr (1998) J Phys Chem 102: 1733
13. Bell RC, Zemski KA, Castleman AW Jr (1998) J Phys Chem A 102: 8293
14. Bell RC, Zemski KA, Castleman AW Jr (1999) J Phys Chem A 103: 2292
15. Bell RC, Zemski KA, Castleman AW Jr (1999) J Phys Chem A 103: 1585
16. Foltin M, Stueber GJ, Bernstein ER (1999) J Chem Phys 111: 9577
17. Martins JBL, Longo E, Andrés J (1993) Int J Quantum Chem 27: 643
18. Martins JBL, Andrés J, Longo E, Taft CA (1995) J Mol Struct (THEOCHEM) 330: 301
19. Sambrano JR, Andrés J, Beltrán A, Sensato F, Longo E (1998) Chem Phys Lett 287: 620
20. Beltrán A, Andrés J, Noury S, Silvi B (1999) J Phys Chem A 103: 3078
21. Calatayud M, Andrés J, Beltrán A, Silvi B (2001) Theor Chem Acc 105: 299
22. Calatayud M, Beltrán A, Andrés J, Silvi B (2001) Chem Phys Lett 333: 493
23. Calatayud M, Beltrán A, Andrés A (2001) J Phys Chem A 105: 9760
24. Becke AD (1993) J Chem Phys 98: 5648
25. Lee C, Yang RG, Parr RG (1988) Phys Rev B 37: 785
26. Frisch MJ, Trucks GW, Schlegel HB, Gill PMW, Johnson BG, Robb MA, Cheeseman JR, Keith T, Peterson GA, Montgomery JA, Raghavachari K, Al-Laham MA, Zakrzewski VG, Ortiz JV, Foresman JB, Cioslowski J, Stefanov BB, Nanayakkara A, Challacombe M, Peng CY, Ayala PY, Chen W, Wong MW, Andres JL, Replogle ES, Gomperts R, Martin RL, Fox DJ, Binkley JS, Defrees DJ, Baker J, Stewart JP, Head-Gordon M, Gonzalez C, Pople JA (1995) Gaussian94, revision B1. Gaussian, Pittsburgh, Pa
27. Boutreau L, Leon E, Luna A, Toulhoat P, Tortajada J (2001) Chem Phys Lett 338: 74
28. Gutsev GL, Rao BK, Jena P (2000) J Phys Chem A 104: 11961
29. Gutsev GL, Rao BK, Jena P, Wang X-B, Wang L-S (1999) Chem Phys Lett 312: 598
30. Gutsev GL, Khanna SN, Rao BK, Jena P (1999) J Phys Chem A 103: 5812
31. Rassolov VA, Pople JA, Ratner MA, Windus TL (1998) J Phys Chem 109: 1223
32. Boys SF, Bernardi F (1970) Mol Phys 19: 553
33. Xantheas SS (1996) J Chem Phys 104: 8821
34. Bader RF (1990) Atoms in molecules. A quantum theory. Clarendon, Oxford
35. Becke AD, Edgecombe KE (1990) J Chem Phys 92: 5397
36. Silvi B, Savin A (1994) Nature 371: 683
37. Noury S, Colonna F, Savin A, Silvi B (1998) J Mol Struct 450: 59
38. Burdett JK, McCormik TA (1998) J Phys Chem A 102: 6366
39. Frisch MJ, Trucks GW, Schlegel HB, Scuseria GE, Robb MA, Cheeseman JR, Zakrzewski VG, Montgomery JA, Stratmann RE, Burant JC, Dapprich S, Millam JM, Daniels AD, Kudin KN, Strain MC, Farkas O, Tomasi J, Barone V, Cossi M, Cammi R, Mennucci B, Pomelli C, Adamo C, Clifford S, Ochterski J, Petersson GA, Ayala PY, Cui Q, Morokuma K, Malick DK, Rabuck AD, Raghavachari K, Foresman JB, Cioslowski J, Ortiz JV, Stefanov BB, Liu G, Liashenko A, Piskorz P, Komaromi I, Gomperts R, Martin RL, Fox DJ, Keith T, Al-Laham MA, Peng CY, Nanayakkara A, Gonzalez C, Challacombe M, Gill PMW, Johnson BG, Chen W, Wong MW, Andres JL, Head-Gordon M, Replogle ES, Pople JA (1998) Gaussian98, revision A.1. Gaussian, Pittsburgh, Pa
40. Noury S, Krokidis X, Fuster F, Silvi B (1997) Topmod package. Paris
41. Pepke E, Murray J, Lyons J, Hwu T-Z (1993) SciAn. Supercomputer Computations Research Institute, Fla
42. Koyanagi GK, Bohme DK, Kretzschmar I, Schröder D, Schwarz H (2001) J Phys Chem A 105: 4259
43. Xu J, Rodgers MT, Griffin JB, Armentrout PB (1998) J Chem Phys 108: 9339
44. Chertihin GV, Bare WD, Andrews L (1997) J Phys Chem A 101: 5090
45. Bader RFW, Johnson S, Tang H, Popelier PLA (1996) J Phys Chem 100: 15398
46. Llusar R, Beltrán A, Andrés J, Noury S, Silvi B (1999) J Comput Chem 20: 1517